

Accelerating Ultrafast Spectroscopy with Compressive Sensing

Sushovit Adhikari,¹ Cristian L. Cortes¹,¹ Xiewen Wen,¹ Shobhana Panuganti¹,² David J. Gosztola¹,¹ Richard D. Schaller,^{1,2} Gary P. Wiederrecht¹,¹ and Stephen K. Gray¹,^{1,*}

¹Center for Nanoscale Materials, Argonne National Laboratory, Lemont, Illinois 60439, USA

²Department of Chemistry, Northwestern University, 2145 Sheridan Road, Evanston, Illinois 60208, USA

(Received 27 July 2020; revised 8 December 2020; accepted 22 December 2020; published 15 February 2021)

Ultrafast spectroscopy is an important tool for studying photoinduced dynamical processes in atoms, molecules, and nanostructures. Typically, the time to perform these experiments ranges from several minutes to hours depending on the choice of spectroscopic method. It is desirable to reduce this time overhead not only to shorten time and laboratory resources, but also to make it possible to examine fragile specimens that quickly degrade during long experiments. In this article, we motivate using compressive sensing to significantly shorten data acquisition time by reducing the total number of measurements in ultrafast spectroscopy. We apply this technique to experimental data from ultrafast transient absorption spectroscopy and ultrafast terahertz spectroscopy and show that good estimates can be obtained with as low as 15% of the total measurements, implying a sixfold reduction in the data acquisition time.

DOI: 10.1103/PhysRevApplied.15.024032

I. INTRODUCTION

Ultrafast spectroscopy has found a wide range of applications to study time-resolved ultrafast dynamical processes [1–5]. Many techniques have been developed spanning different time and photon energy ranges, including ultrafast transient absorption spectroscopy, time-resolved photoelectron spectroscopy, multidimensional spectroscopy, and terahertz spectroscopy [6,7]. These techniques can be very time consuming with acquisition times varying drastically depending on the method. Reducing the time overhead is important, not only for efficiency, but also for making it possible to examine specimens that degrade quickly due to prolonged exposure to a laser beam.

Here we show how to significantly shorten the duration of ultrafast spectroscopy experiments with compressive sensing. We apply compressive sensing to two important ultrafast techniques: ultrafast transient absorption spectroscopy and ultrafast terahertz spectroscopy. The specimen chosen for the transient absorption is colloidal solution of 50 nm diameter TiN nanoparticles in water, which are of growing interest as refractory metal nanostructures resistant to heat or optical damage for plasmonic applications [8]. This specimen was chosen due to its high degree of optical scattering, which makes it extremely challenging and very time consuming to acquire data with a reasonable signal-to-noise ratio. For our experiment, the data acquisition time was about 4 h. For ultrafast terahertz spectroscopy, measurements are performed on a

methylammonium lead iodide (MAPbI_3) thin film that is spin casted on quartz. This material class is of interest for solar energy conversion and is believed to exhibit long carrier lifetimes owing to low-frequency lattice deformations that may help screen charges. The data acquisition for a full two-dimensional (2D) time-resolved terahertz experiment took about 7 h to complete, and could require more time for a higher signal-to-noise ratio. These conditions challenge the stability of both laser systems and many specimens. To overcome these difficulties we show that, by taking sparse, random measurements in time, thereby taking a fraction of the total measurements compared to conventional experiments, compressive sensing can faithfully reconstruct the full experimental result.

II. COMPRESSIVE SENSING FOR ULTRAFAST SPECTROSCOPY EXPERIMENTS

Recently, there has been wide interest in using different techniques to speed up optical experiments [9–13]. Compressive sensing (CS) is one such technique for efficiently acquiring and reconstructing signals [14–17]. It has successfully been applied in many fields, including magnetic resonance imaging, fluorescence microscopy, multidimensional nuclear magnetic resonance spectroscopy, quantum imaging, and quantum tomography [18–27]. CS has also been used in multidimensional spectroscopy for applications in chemistry with impressive speed ups shown [28–30]. We propose compressive sensing for material science and condensed matter physics where a different set of ultrafast spectroscopic methods are used, such as transient absorption and ultrafast terahertz spectroscopy. We hope

*gray@anl.gov

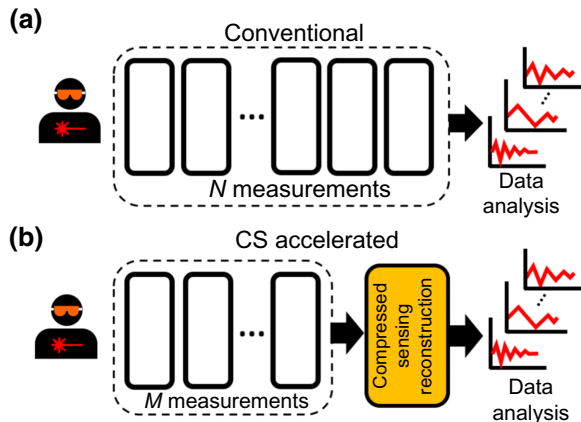


FIG. 1. Comparison between conventional and CS-accelerated experiments. (a) shows a conventional experiment which requires N measurements for the fully resolved result. (b) shows the CS-accelerated scheme with $M \ll N$ measurements to yield an estimate of the fully resolved result.

that our work helps bridge the gap between the CS community and the ultrafast spectroscopy community where advanced algorithmic methods are not commonly used.

In Fig. 1 we depict the basic approach. Generally, the number of measurements N to capture full information of a signal is determined by the Nyquist-Shannon sampling theorem: the sampling rate should be at least twice the highest frequency of the signal, $2f_{\max}$ [31]. If some maximum time T is required to observe the dynamics or infer a spectrum of a given resolution, then $N = T/\Delta t = 2f_{\max}T$ total measurements would be needed, with Δt being the time between measurements (inverse sampling rate). (This latter analysis is correct if one only has an upper limit for f_{\max} and *no* other knowledge about the signal.) In this sampling limit one achieves a response or spectrum that is what we term a fully resolved result. CS overcomes this limit by invoking a sparsity assumption of the signal in some known basis. When a signal is transformed to this basis, most of the coefficients are negligibly small. The existence of such a basis can be used to significantly reduce the total number of measurements required to reconstruct the full signal. Many natural signals are sparse in the Fourier domain. Since time-domain signals are usually real, the discrete cosine transform (DCT) [32] is widely used for compression and CS reconstruction. Other transformations, such as Haar, total variation, and Hadamard transformations are also widely used [12,33,34].

CS reconstructs a signal by solving the convex optimization problem

$$\min_{\tilde{x}} \|\tilde{x}\|_1 \quad \text{subject to} \quad A\tilde{x} = y. \quad (1)$$

Here, $\tilde{x} = \psi x$ is the $N \times 1$ sparse solution vector and ψ is the transformation matrix that takes the signal x (e.g., transient absorption) to a sparse basis. We use the DCT and

Haar and Hadamard transformations as possible choices for ψ . Here $\|\cdot\|_1$ is the l_1 norm, i.e., the sum of the absolute values of the components of \tilde{x} . The most sparse solution is given by minimizing the number of nonzero components of the solution vector's \tilde{x} or l_0 norm. However, l_0 minimization is nonconvex and falls under *NP-hard* computational complexity, which is very difficult to solve. Here y is the $M \times 1$ vector representing the small number ($M \ll N$) of random measurements taken in the experiment; $A = \phi\psi^{-1}$ is a $M \times N$ matrix, with ϕ representing a $M \times N$ random measurement matrix, which we take to be a submatrix of the $N \times N$ identity matrix with M rows chosen randomly. For a K -sparse signal, having K nonzero coefficients, the above optimization problem is able to faithfully reconstruct the signal with $\mathcal{O}(K \log(N/K))$ with high probability. In essence, if K is much smaller than N , this means that on the order of $\log N$ measurements, as opposed to N measurements, suffice.

Remarkably, it has been shown that no reconstruction algorithm can reconstruct the signal with substantially fewer measurements [16]. Additional details of this algorithm are specified in Sec. V.

To see why the CS is well suited to ultrafast spectroscopy, consider a pump-probe framework, typical of many such experiments. A short pump pulse centered at time t_0 excites a specimen and a probe pulse at various later times $t = t_0 + \tau$ is used to measure the evolution of some material response, \mathcal{R} (e.g., absorbance or transmittance) [7]:

$$\mathcal{R}(\tau) = \mathcal{R}_{-\infty} + \Delta\mathcal{R}(\tau) \quad (2)$$

with $\mathcal{R}_{-\infty}$ the material response prior to the pump. Many measurements are taken at various probe time delays τ , giving information about the full dynamics. Such ultrafast experiments can be time consuming due to the need of making repeated measurements with small increments in $\Delta\tau$. CS is ideally suited for ultrafast optics because in a wide variety of material systems, $\mathcal{R}(\tau)$ is often dominated by a small number, or small range, of frequencies, implying the existence of a sparse basis. For many systems, the total number of measurements taken in conventional ultrafast experiments far outweigh the actual number of measurements, approximately $K \log(N/K)$, required by CS theory. Here, we test the performance of CS signal reconstruction for two prototypical experiments: ultrafast transient absorption and ultrafast terahertz spectroscopy.

III. RESULTS

A. Ultrafast transient absorption spectroscopy

An ultrafast transient absorption spectroscopy is a pump-probe experiment in which a specimen is excited with a femtosecond pump pulse, followed by a probe pulse with a variable time delay. The changes in transmittance or

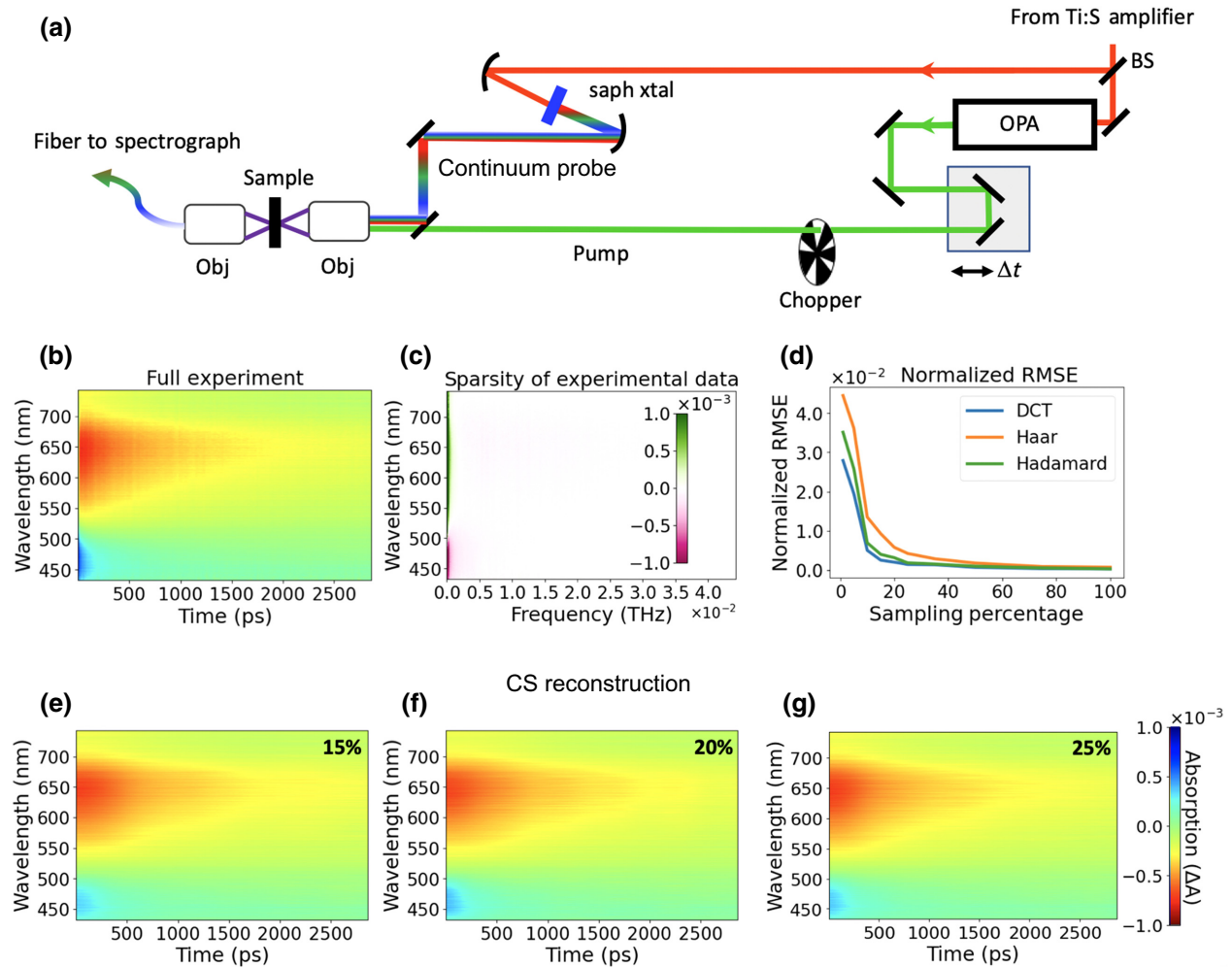


FIG. 2. Ultrafast transient absorption spectroscopy. Panel (a) shows a schematic of the experimental setup. The terms saph xtal, OPA and BS denote sapphire crystal, optical parametric amplifier, and beam splitter, respectively. Panel (b) shows the observed change in absorbance across different wavelengths. In panel (c) we demonstrate that the full experimental data is very sparse in the DCT domain. This allows CS to reconstruct signals with a fraction of the measurements of a conventional experiment. In (d) we plot the normalized root-mean-square error for DCT, Haar, and Hadamard as a function of the sampling percentage. Panels (e)–(g) show the CS reconstruction with 15%, 20%, and 25% samples, respectively.

absorbance over various time delays are measured, giving information about the properties of the specimen. Transient absorption spectroscopy has been used to characterize an extraordinarily large range of photoinduced dynamical processes, ranging from molecular excited states, electronic transitions in nanoparticles, plasmonics, charge separation, and transport phenomena, to name just a few [35–37].

A schematic of our ultrafast transient absorption spectroscopy experiment is shown in Fig. 2. The output of an amplified femtosecond laser system (Spectra Physics Tsunami and Spitfire) operating at 5 kHz and 800 nm pumps an optical parametric amplifier to create wavelength tunable 130 fs pulses. We select the pump pulses to have a central wavelength of 900 nm, chosen to excite the lower

energy side of the broad plasmon band of the TiN nanoparticles centered at 650 nm, and outside the visible probe spectral region in order to avoid additional pump scattering noise. The measured 650 nm plasmon resonance center is consistent with the literature [8]. A small portion of the 800 nm amplified light (5%) is focused into a thin (2 mm) sapphire crystal to create a continuum probe. The pump beam is chopped at half the repetition rate to create “pump on” and “pump off” such that a transient absorption signal can be measured with each pump pair. With variable delay of the probe relative to the pump, time-resolved transient absorption spectroscopy can be acquired. The pump and probe beams are focused and spatially overlapped in the specimen (TiN nanoparticles in water). The visible spectral range is measured simultaneously for each delay. The

probe light is then fiber-optically coupled to a multichannel spectrograph where the full continuum in the visible spectral range is measured simultaneously for each delay. (The spectrograph uses a 1024 channel CMOS detector with high-speed 16-bit digitizing electronics that allow the entire spectrum to be read out at 5 kHz.) For this data, each delay required tens of thousands of transient absorption pump-pair measurements. The full data acquisition took 4 h due to the high scattering of the colloidal nanoparticle specimen. Next, we show how CS can drastically shorten the duration of experiment.

In Fig. 2(b) we display the full experimental data showing the change in absorbance (ΔA) across different wavelengths. It can be seen that ΔA varies with wavelength. The data indicate a strong transient response of the TiN plasmon absorption following photoexcitation. Since the transient absorption measurement is a difference measurement, it is possible to get positive (an absorption with less light transmitted through the specimen) and negative transient absorption signals (typically, a bleach of the ground-state absorption, with more light transmitted through the specimen), particularly when there is a spectral shift in the excited nanostructure. In Fig. 2(b), the data indicate that the plasmon resonance of the TiN nanoparticles, centered at 650 nm, is bleached upon photoexcitation. The blue part of the spectral region, below 500 nm and lying at a higher photon energy than the plasmon resonance, begins to show weak transient absorption features, likely due to the pump-induced absorption of bound electronic transitions. In Fig. 2(c) we show the sparsity of the full experimental data for each wavelength in the DCT domain. We can clearly see that the signal is sparse with almost all components concentrated near zero frequency. (See Fig. S1 of the Supplemental Material [38] for an expanded view of the low-frequency regime.) In fact, only about 5% of the frequency coefficients contain almost all the information about the signal. This suggests that CS can reconstruct the signal with about 15% of the measurements of a conventional experiment. In Figs. 2(e)–2(g) we show the CS reconstruction at 15%, 20%, and 25%, respectively. Qualitatively, all these CS reconstructions look very similar to the full result in Fig. 2(b). This also corroborates our assumption that about 15% of the measurements of a conventional experiment are sufficient to reconstruct the full experimental signal. To quantify the overall signal reconstruction, we compare the normalized root-mean-square error for different sampling percentages in Fig. 2(d). The normalized root-mean-square error (see Sec. V) in this case is defined to be the usual root-mean-square error (RMSE) of the CS fit to the full set of experimental results over all probe pulse times and wavelengths divided by the range of the signal, i.e., the overall maximum minus the overall minimum of the absorbance change. The normalized RMSE (as opposed to the RMSE) can be a rough gauge for comparing qualities of fits for different types

of experimental results. We also compare the DCT with Haar and Hadamard transforms. The DCT performs best among these transformations, followed by Hadamard and Haar transforms. It is interesting to note that the normalized RMSE drops quickly and does not change much from 15% for higher sampling percentages. This suggests that a number of measurements as low as 15% of that of a conventional experiment is sufficient for a fair reconstruction (i.e., one achieving 0.01–0.02 normalized RMSE or better) of the signal. At the other extreme of 100% sampling, note that the normalized RMSE in Fig. 2(d), while quite small, does not reach exactly zero. The reason for this is that the CS procedure represents a compromise between fitting the data and keeping the signal sparse via an additional regularization term (see Sec. V). This latter term can prevent perfect fitting at 100% sampling.

B. Ultrafast terahertz spectroscopy

Ultrafast terahertz spectroscopy is another useful technique for investigating specimens with short pulses of terahertz radiation. It is used for examining spectral responses of a specimen in the far infrared and can exhibit sensitivity to pump-induced optical conductivity as well as phonon dynamics in some cases [39,40]. Measurement of the terahertz spectral response is accomplished using electro-optical sampling wherein a time delayed 800 nm laser pulse is spatially overlapped with the terahertz pulse in a GaP or ZnTe crystal to evaluate the terahertz waveform by scanning temporal delay (Δt_2). As such, ultrafast terahertz spectroscopy can necessitate two dimensions of scanning that increases the data acquisition time.

A schematic of ultrafast terahertz spectroscopy is shown in Fig. 3(a). In our experiment, we probe a methylammonium lead iodide (MAPbI₃) thin film on quartz at 80 K relative to a 500 nm pump pulse with time delay Δt_1 . Terahertz probe pulses are produced via optical rectification in a 300 μ m thick GaP(110) crystal. Absorption of 500 nm pump photons produces electron-hole pairs in the MAPbI₃ specimen that alter the conductivity of the film and change transparency to the terahertz probe pulse. A recent literature report conveys other physical phenomena in this material, including altered optical access to Rydberg states as well as phonon evolution [40].

In Fig. 3(b) we show the acquired experimental data. Here, the pump-induced change in the transmitted terahertz probe intensity is plotted following optical excitation, where photogenerated carriers alter the sample conductivity owing to the light-induced production of highly polarizable charge carriers and phonon population evolution. In particular, the long carrier lifetimes and diffusion lengths in this material may result from lattice distortions and low-frequency vibrational modes, which can be interrogated via this method. In Fig. 3(c) we demonstrate the sparsity of the full experimental result in the DCT

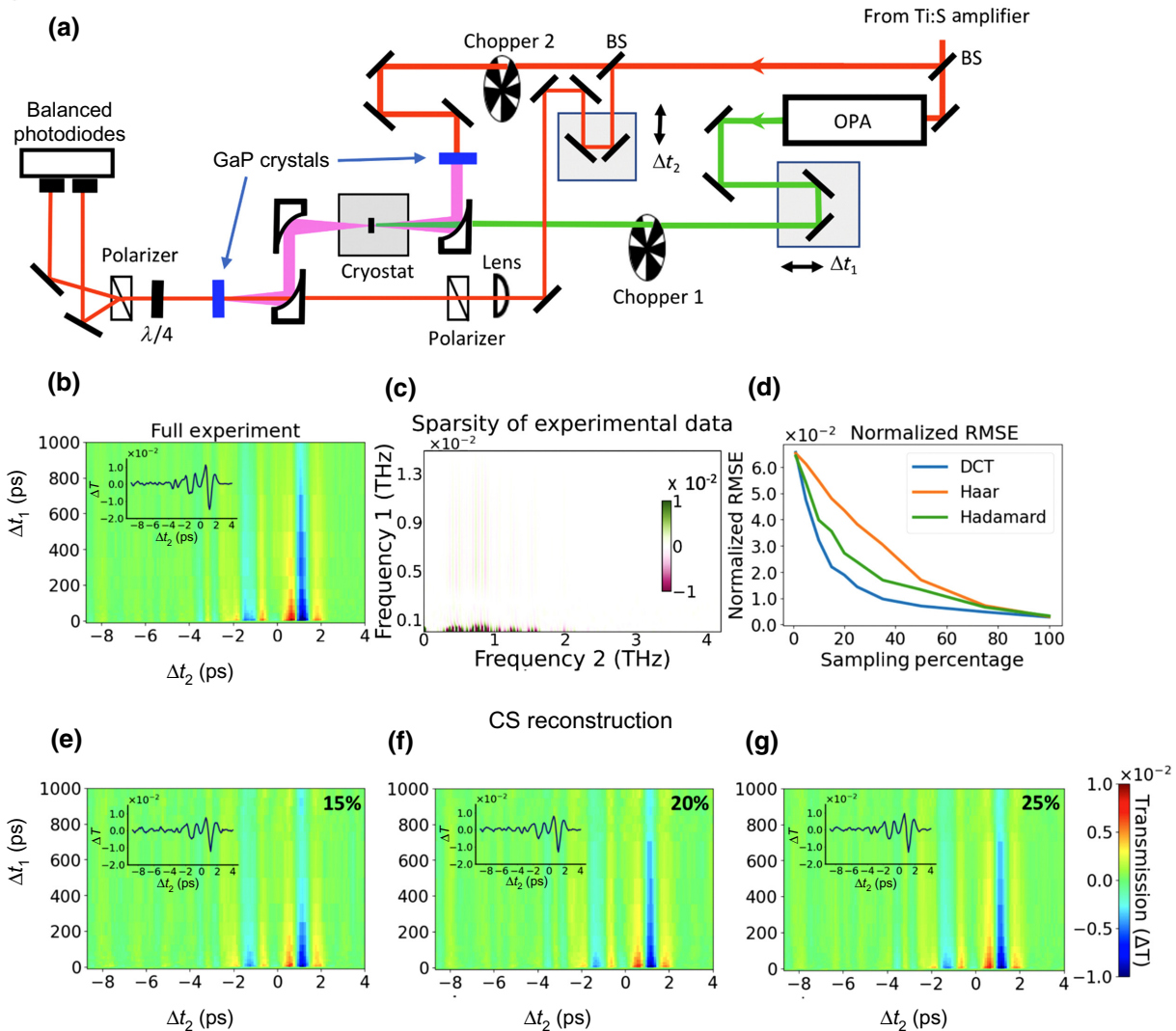


FIG. 3. Ultrafast terahertz spectroscopy. Panel (a) shows the schematic of the experimental setup. The terms OPA and BS denote optical parametric amplifier and beam splitter, respectively. (b) Change in transmitted terahertz probe intensity as a function of pump pulse application time Δt_1 and electro-optical sampling probe delay time Δt_2 . The inset here and those in panels (e)–(g) show a typical profile in Δt_2 for a fixed $\Delta t_1 = 30$ ps. In (c) we show the sparsity of the signal in the DCT domain. Almost all the information is contained in about 7% of the frequency coefficients. This allows CS to reconstruct the full signal with a fraction of the measurements of a conventional experiment. In (d) we show a comparison between normalized RMSE for DCT, Haar, and Hadamard as a function of the sampling percentage. In (e)–(g) we show the CS reconstruction with 15%, 20%, and 25% samples, respectively.

domain. As before, the fact that the signal is sparse in the DCT domain is the key point that allows us to use compressed sensing for reconstructing the full signal with about 18% of the measurements of a conventional experiment. In Figs. 3(e)–3(f) we show the CS reconstruction with different percentage measurements (15%, 20%, and 25%). These CS reconstructions look very similar to the full experimental result in Fig. 3(b). Again, it verifies our assumption that about 18% of the measurements of a conventional experiment reconstruct the full signal. As before, for quantitative assessment, in Fig. 3(d) we show the normalized RMSE for DCT and Hadamard and Haar

transforms. The definition we employ for the normalized RMSE in these ultrafast terahertz measurements (see Sec. V) is similar to what we used for the transient absorption measurements, i.e., we simply normalize the usual RMSE by the range of the entire 2D signal. We find from Fig. 3(d) that the corresponding normalized RMSE values for a good description of the experimental data is approximately 1×10^{-2} , within about a factor of 2 of the transient absorption case of Fig. 2(d) (2×10^{-2}). We observe a similar trend as in the case of ultrafast transient absorption spectroscopy. The DCT performs best among these transformations. Also, the magnitude of the changes in

normalized RMSE above 20% sampling is small, i.e., less than 0.01, suggesting that a sampling range of 15% to 25% gives a good estimate (normalized RMSE values of 0.01–0.02 or better) of the full signal.

The sampling fraction sufficient for reconstruction is $cK \log(N/K)/N$, where c is a problem-dependent proportionality constant. We estimate from the transforms of the full data that K/N is approximately 0.04 in both the transient absorption and terahertz experiments. If c is the same for both types of experiments then one would expect the same sampling percentages. We find that the required sampling percentage for the terahertz case is just a little higher (18%) compared to the transient absorption case (15%) and, we would argue, not particularly inconsistent with the expectation.

IV. DISCUSSION

We have provided here proof of principle that, for ultrafast spectroscopy experiments on nanoscale materials, as little as 15% of the data typically acquired can be used to obtain good reconstructions of the relevant responses using CS. An important proviso to note, however, is that early time responses that feature fine structure, such as the coherent nonresonant response noted in the Supplemental Material [38] (Fig. S2), cannot be resolved with the present approach and a finer time scan for early times would be required to see it, with CS being more appropriate for describing the later times. Whether or not more or less data are needed for other types of samples and/or experiments depends entirely on the nature (sparsity) of the underlying signals. Furthermore, our analysis is based on knowledge of the fully resolved system response. If our approach is to become useful in a practical context, it must of course be implemented in scenarios wherein the fully resolved response is not known. One approach would be to perform a real-time CS reconstruction for every experimental data point, or set of experimental data points, that is sequentially acquired. For example, we can have a CS reconstruction for n data points, then another CS reconstruction for $n + 1$ data points. We can then compare the two CS reconstructions using a distance metric, e.g., the l_2 norm, and if it falls below a certain threshold, the experiment is stopped. Fully flushing out this approach, e.g., determining suitable sampling and stopping criteria for this procedure, and demonstrating that it works in an experimental context represents an important next step for our result here to be of practical significance. Furthermore, while our analysis of actual experimental data suggests that 15%–20% sampling should suffice for signal reconstruction, noisier data could compromise this conclusion and a detailed analysis of the effect of noise represents another important future direction to explore.

It should also be pointed out that numerous other procedures than the CS approach presented here can be devised

that can reduce the amount of data acquisition required and some could yield equally good results. Collection of data as described above, with some concentration on short times and less concentration on long times coupled with simple linear or some other low-order interpolation is one approach. Fitting physical models based on the known or expected physics and chemistry (e.g., sums of exponentials representing various possible relaxation processes) could, if applicable, lead to even more substantial savings. The CS approach discussed here has the advantage that it is well founded with a substantial amount of applied mathematics literature behind it, and it has numerous demonstrated successes. It is also the case that, as one goes beyond 1D and 2D imaging, the CS approach may offer advantages (see, e.g., Ref. [41]).

We envision this technique will be very beneficial in many ultrafast spectroscopy experiments, where data acquisition is time consuming due to raster scanning. For example, in many experiments, a raster scan along temperature or voltage is required. With temperature or voltage as one axis and, say, probe delay time for a fixed wavelength (or possibly a third dimension also involving wavelength) as another axis, the signal may still be sparse and our approach valid, significantly reducing the number of required measurements. Of course, measurements at these different temperature or voltage values are required. Our method will also provide significant speedup for higher-dimensional ultrafast spectroscopy by reducing the number of measurements in each dimension. Moreover, it should also make it possible to measure fragile specimens that degrade on long exposure under the laser.

V. METHODS

A. Compressive sensing

One way of solving Eq. (1) is by formulating it as a “Lasso” functional or “basis pursuit denoising” problem as [42,43]

$$\min_{\tilde{x}} \frac{1}{2} \|A\tilde{x} - y\|_2^2 + \lambda \|\tilde{x}\|_1. \quad (3)$$

As with Eq. (1), \tilde{x} can be thought of as a $N \times 1$ vector, and the sampled signal for CS, y , is $M \times 1$ with $M \ll N$. In general, lacking detailed knowledge of the sparsity of \tilde{x} , and of course not knowing the true fully resolved signal, which will be the case for most applications, it is difficult to determine what M should be without some experimentation, e.g., taking additional measurements (increasing M) and looking for reasonably converged signal predictions. See also Sec. IV. For the ultrafast applications studied here, we find empirically that M/N in the 0.2–0.25 range, i.e., 20%–25% sampling, can lead to adequate CS reconstructions.

The above optimization problem can be seen as a trade-off between minimizing the squared error (i.e. making $A\tilde{x}$

as close to y) and finding \tilde{x} with a minimal l_1 norm. Here, λ is a regularization parameter that controls the trade-off between sparsity and reconstruction fidelity. Cross validation [44] is often recommended for determining this parameter and this is the approach we take. We typically hold out about 20% of the sampled M points and carry out CS on the remaining sampled points for various values of λ . As with choosing M , there is no simple rule for choosing the number of points to be held out in cross validation. The optimal λ is then the one that leads to the smallest mean-square error between the CS predictions of the held-out points and their actual values. Note that in the transient absorption CS analysis, we determine the optimal λ once for a midrange wavelength, finding that this procedure suffices to give good CS reconstructions. In the case of the terahertz measurements, since the data is fully 2D, only one determination of the optimal λ is necessary. See also the Supplemental Material [38].

There are also other cross-validation approaches than the above very simple, single set hold-out strategy that could be considered. For example, one could divide the data into K subsets and carry out CS reconstructions for the K possible data sets corresponding to the data with one of the subsets removed [44]. One would then compute the average error across all these subset removal cases. Minimization of this error with respect to varying λ would then yield the optimal λ for CS reconstruction. This latter procedure, while more balanced and likely better in terms of achieving good reconstructions, is also more open ended (e.g., in choosing the size of K) and much more time consuming than the simple hold-out strategy we adopt. Some alternatives to cross validation are also discussed in Ref. [45].

B. Data preprocessing and normalized RMSE

Before applying CS on the experimental data we preprocess the full data, excluding some regions for reasons to be explained and interpolating to lead to evenly spaced data sets of convenient sizes for analysis. The interpolation is not necessary for CS reconstruction in general, but we want to compare CS reconstructions with different transformations (DCT, Hadamard, and Haar), and the Haar and Hadamard transformations require an input signal with its number of components being a power of two.

In the case of the transient absorption measurements, the initial data consists of the transmittance as a function of 273 different wavelengths ranging from 421 to 743 nm and 255 pulse times collected from $t = -5$ to $t = 2870$ ps. The 421 to 431 nm data are very noisy and we exclude them from the analysis, leading to $N_1 = 263$ wavelengths. This wavelength range is excluded because of the very small amount of continuum photons generated by 800 nm light incident on the sapphire crystal. Very low levels of light in the probe beam cause large digitization noise in

the measured signal. We also observe a coherent nonresonant response of the solvent at $t = 0$ and we exclude this region in subsequent analysis (see the Supplemental Material [38] for details). After excluding this anomalous region, we interpolate the data such that each wavelength has $N_2 = 256$ pulse times. In terms of experiments, this would correspond to fewer measurements at these random times, whereas in a conventional experiment, many more measurements are taken with a fine increment in time delays.

In the case of the ultrafast terahertz measurements, the initial data is comprised of 26 and 151 scans along Δt_1 and Δt_2 , respectively, with Δt_1 ranging from -10 to 1000 ps and Δt_2 ranging from -8.7 to 4 ps. We interpolate this data to obtain $N_1 = 32$ and $N_2 = 128$ evenly spaced points in Δt_1 and Δt_2 .

In both cases, we choose points randomly from the original experimental data sets (excluding some regions as discussed above) to define reduced data sets to perform CS reconstructions on. Note that these experimental data sets tend to have finer time steps at shorter times owing to the short times exhibiting some rapid variations and so the samplings are therefore not distributed evenly in time and reflect the increased importance of the shorter times. Note that our study benefits from prior knowledge of the full signals, which allows us to perform a variety of tests to establish guidelines for successful reconstructions. In actual experiments where the method would be deployed in order to reduce experimental effort, the various random pulse times (both the single-probe and the two-probe cases) could be generated in advance and programmed into the computer controlling the experiments. In order to assess the accuracy of the CS reconstructions, for both the ultrafast transient absorption and terahertz measurements, we use the normalized RMSE,

$$s_n = \frac{1}{x_{\max} - x_{\min}} \sqrt{\frac{\sum_{i,j} (\tilde{x}_{i,j} - x_{i,j})^2}{N_1 N_2}} \quad (4)$$

with \tilde{x} being the CS reconstruction, x being a $N_1 \times N_2$ sample of the experimental data, and x_{\max} and x_{\min} being the maximum and minimum values of the experimental data. The normalized RMSE is averaged over 10 runs, which corresponds to uniquely sampled data on each run.

ACKNOWLEDGMENTS

This material is based on work supported by Laboratory Directed Research and Development (LDRD) funding from Argonne National Laboratory, provided by the Director, Office of Science, of the U.S. Department of Energy under Contract No. DE-AC02-06CH11357. Use of the Center for Nanoscale Materials, an Office of Science user facility, was supported by the U.S. Department of Energy,

Office of Science, Office of Basic Energy Sciences, under Contract No. DE-AC02-06CH11357. We thank Alexander Govorov for useful discussions.

-
- [1] Margherita Maiuri, Marco Garavelli, and Giulio Cerullo, Ultrafast spectroscopy: State of the art and open challenges, *J. Am. Chem. Soc.* **142**, 3 (2020).
- [2] Neil T. Hunt, 2D-IR spectroscopy: Ultrafast insights into biomolecule structure and function, *Chem. Soc. Rev.* **38**, 1837 (2009).
- [3] Gavin D. Reid and Klaas Wynne, in *Encyclopedia of Analytical Chemistry*, edited by R. A. Meyers (Chichester, John Wiley & Sons, 2000), pp. 13644–13670.
- [4] Rudi Berera, Rienk van Grondelle, and John T. M. Kennis, Ultrafast transient absorption spectroscopy: Principles and application to photosynthetic systems, *Photosyn. Res.* **101**, 105 (2009).
- [5] Peter M. Kraus, Michael Zürch, Scott K. Cushing, Daniel M. Neumark, and Stephen R. Leone, The ultrafast x-ray spectroscopic revolution in chemical dynamics, *Nat. Rev. Chem.* **2**, 82 (2018).
- [6] Jagdeep Shah, *Ultrafast Spectroscopy of Semiconductors and Semiconductor Nanostructures*, 2nd Enlarged Edition (Springer, Berlin, 1999).
- [7] Andrew Weiner, *Ultrafast Optics* (John Wiley & Sons, Hoboken, New Jersey, 2009).
- [8] Urcan Guler, Sergey Suslov, Alexander V. Kildishev, Alexandra Boltasseva, and Vladimir M. Shalaev, Colloidal plasmonic titanium nitride nanoparticles: Properties and applications, *Nanophotonics* **4**, 269 (2015).
- [9] Cristian L. Cortes, Sushovit Adhikari, Xuedan Ma, and Stephen K. Gray, Accelerating quantum optics experiments with statistical learning, *Appl. Phys. Lett.* **116**, 184003 (2020).
- [10] Chenglong You, Mario A. Quiroz-Juárez, Aidan Lambert, Narayan Bhalsal, Chao Dong, Armando Perez-Leija, Amir Javaid, Roberto de J. León-Montiel, and Omar S. Magaña-Loaiza, Identification of light sources using machine learning, *Appl. Phys. Rev.* **7**, 021404 (2020).
- [11] Zhaxylyk A. Kudyshev, Simeon Bogdanov, Theodor Isaacsson, Alexander V. Kildishev, Alexandra Boltasseva, and Vladimir M. Shalaev, Rapid classification of quantum sources enabled by machine learning, *Adv. Quantum Technol.* **3**, 2000067 (2020).
- [12] Gregory A. Howland, P. Ben Dixon, and John C. Howell, Photon-counting compressive sensing laser radar for 3D imaging, *Appl. Opt.* **50**, 5917 (2011).
- [13] E. M. Simmernan, H.-H. Lu, A. M. Weiner, and J. M. Lukens, Efficient compressive and bayesian characterization of biphoton frequency spectra, *Opt. Lett.* **45**, 2886 (2020).
- [14] Richard G. Baraniuk, Compressive sensing [lecture notes], *IEEE Signal Process. Mag.* **24**, 118 (2007).
- [15] Emmanuel J. Candès and Michael B. Wakin, An introduction to compressive sampling, *IEEE Signal Process. Mag.* **25**, 21 (2008).
- [16] David L. Donoho, Compressed sensing, *IEEE Trans. Inf. Theory* **52**, 1289 (2006).
- [17] Emmanuel J. Candès, Justin K. Romberg, and Terence Tao, Stable signal recovery from incomplete and inaccurate measurements, *Commun. Pure Appl. Math.: A J. Issued Courant Inst. Math. Sci.* **59**, 1207 (2006).
- [18] Yan Yang, Jian Sun, Huibin Li, and Zongben Xu, in *Advances in Neural Information Processing Systems*, edited by D. Lee, M. Sugiyama, U. Luxburg, I. Guyon, and R. Garnett (Curran Associates, Inc., 2016), Vol. 29, p. 10.
- [19] Vincent Studer, Jérôme Bobin, Makhlad Chahid, Hamed Shams Mousavi, Emmanuel Candès, and Maxime Dahan, Compressive fluorescence microscopy for biological and hyperspectral imaging, *Proc. Natl. Acad. Sci.* **109**, E1679 (2012).
- [20] Krzysztof Kazimierczuk and Vladislav Yu Orehov, Accelerated NMR spectroscopy by using compressed sensing, *Angew. Chem. Int. Ed.* **50**, 5556 (2011).
- [21] Gregory A. Howland and John C. Howell, Efficient High-Dimensional Entanglement Imaging with a Compressive-Sensing Double-Pixel Camera, *Phys. Rev. X* **3**, 011013 (2013).
- [22] Vladimir Katkovnik and Jaakko Astola, Compressive sensing computational ghost imaging, *JOSA A* **29**, 1556 (2012).
- [23] A. Shabani, R. L. Kosut, M. Mohseni, H. Rabitz, M. A. Broome, M. P. Almeida, A. Fedrizzi, and A. G. White, Efficient Measurement of Quantum Dynamics via Compressive Sensing, *Phys. Rev. Lett.* **106**, 100401 (2011).
- [24] David Gross, Yi-Kai Liu, Steven T. Flammia, Stephen Becker, and Jens Eisert, Quantum State Tomography via Compressed Sensing, *Phys. Rev. Lett.* **105**, 150401 (2010).
- [25] Petros Zerom, Kam Wai Clifford Chan, John C. Howell, and Robert W. Boyd, Entangled-photon compressive ghost imaging, *Phys. Rev. A* **84**, 061804 (2011).
- [26] Ori Katz, Yaron Bromberg, and Yaron Silberberg, Compressive ghost imaging, *Appl. Phys. Lett.* **95**, 131110 (2009).
- [27] Xiewen Wen, Sushovit Adhikari, Cristian L. Cortes, David J. Gosztola, Stephen K. Gray, and Gary P. Wiederrecht, Ghost imaging second harmonic generation microscopy, *Appl. Phys. Lett.* **116**, 191101 (2020).
- [28] Xavier Andrade, Jacob N. Sanders, and Alán Aspuru-Guzik, Application of compressed sensing to the simulation of atomic systems, *Proc. Natl. Acad. Sci.* **109**, 13928 (2012).
- [29] Jacob N. Sanders, Semion K. Saikin, Sarah Mostame, Xavier Andrade, Julia R. Widom, Andrew H. Marcus, and Alán Aspuru-Guzik, Compressed sensing for multidimensional spectroscopy experiments, *J. Phys. Chem. Lett.* **3**, 2697 (2012).
- [30] Josef A. Dunbar, Derek G. Osborne, Jessica M. Anna, and Kevin J. Kubarych, Accelerated 2D-IR using compressed sensing, *J. Phys. Chem. Lett.* **4**, 2489 (2013).
- [31] Thomas M. Cover and Joy A. Thomas, *Elements of Information Theory*, 2nd Edition (John Wiley & Sons, Hoboken, New Jersey, 2006).
- [32] G. Strang, The discrete cosine transform, *SIAM Rev.* **41**, 135 (1999).
- [33] Fernando Soldevila, Esther Irles, V. Durán, P. Clemente, Mercedes Fernández-Alonso, Enrique Tajahuerce, and

- Jesús Lancis, Single-pixel polarimetric imaging spectrometer by compressive sensing, *Appl. Phys. B* **113**, 551 (2013).
- [34] Chengbo Li, Master's thesis, Rice University, 2010.
- [35] Lili Wang, Christopher McCleese, Anton Kovalsky, Yixin Zhao, and Clemens Burda, Femtosecond time-resolved transient absorption spectroscopy of $\text{CH}_3\text{NH}_3\text{PbI}_3$ perovskite films: Evidence for passivation effect of PbI_2 , *J. Am. Chem. Soc.* **136**, 12205 (2014).
- [36] Stephanie R. Pendlebury, Monica Barroso, Alexander J. Cowan, Kevin Sivula, Junwang Tang, Michael Grätzel, David Klug, and James R. Durrant, Dynamics of photogenerated holes in nanocrystalline $\alpha\text{-Fe}_2\text{O}_3$ electrodes for water oxidation probed by transient absorption spectroscopy, *Chem. Commun.* **47**, 716 (2011).
- [37] Giulia Grancini, Dario Polli, Daniele Fazzi, Juan Cabanillas-Gonzalez, Giulio Cerullo, and Guglielmo Lanzani, Transient absorption imaging of P3HT:PCBM photovoltaic blend: Evidence for interfacial charge transfer state, *J. Phys. Chem. Lett.* **2**, 1099 (2011).
- [38] See Supplemental Material at <http://link.aps.org supplemental/10.1103/PhysRevApplied.15.024032> for further details on the CS procedures and results.
- [39] Charles A. Schmuttenmaer, Exploring dynamics in the far-infrared with terahertz spectroscopy, *Chem. Rev.* **104**, 1759 (2004).
- [40] Liang Luo, Long Men, Zhaoyu Liu, Yaroslav Mudryk, Xin Zhao, Yongxin Yao, Joong M. Park, Ruth Shinar, Joseph Shinar, Kai-Ming Ho, Ilias E. Perakis, Javier Vela, and Jigang Wang, Ultrafast terahertz snapshots of excitonic rydberg states and electronic coherence in an organometal halide perovskite, *Nat. Commun.* **8**, 15565 (2017).
- [41] S. Ganguli and H. Sompolinsky, Compressed sensing, sparsity, and dimensionality in neuronal information processing and data analysis, *Annu. Rev. Neurosci.* **35**, 485 (2012).
- [42] Robert Tibshirani, Regression shrinkage and selection via the lasso, *J. R. Stat. Soc.: Ser. B (Methodological)* **58**, 267 (1996).
- [43] Scott Shaobing Chen, David L. Donoho, and Michael A. Saunders, Atomic decomposition by basis pursuit, *SIAM Rev.* **43**, 129 (2001).
- [44] X. Huan, C. Safta, K. Sargsyan, Z. P. Vane, G. Lacaze, J. C. Oelelein, and H. N. Najm, Compressive sensing with cross-validation and stop-sampling for sparse polynomial chaos expansions, *SIAM/ASA J. Uncertainty Quantification* **6**, 907 (2008).
- [45] A. Shchukina, P. Kasprzak, R. Dass, M. Nowakowski, and K. Kazimierczuk, Pitfalls in compressed sensing reconstruction and how to avoid them, *J. Biomol. NMR* **68**, 79 (2017).